

Article

Promotional Effect of Manganese on Selective Catalytic Reduction of NO by CO in the Presence of Excess O₂ over M@La-Fe/AC (M = Mn, Ce) Catalyst

Fatemeh Gholami ^{1,*}, Zahra Gholami ^{2,*}, Martin Tomas ¹, Veronika Vavrunkova ¹, Somayeh Mirzaei ³ and Mohammadtaghi Vakili ⁴

¹ New Technologies—Research Centre, University of West Bohemia, 30100 Plzeň, Czech Republic; mtomas@ntc.zcu.cz (M.T.); vavrunko@ntc.zcu.cz (V.V.)

² Unipetrol Centre of Research and Education, a.s, Areál Chempark 2838, Záluží 1, 43670 Litvínov, Czech Republic

³ Department of Chemical Engineering, National Yulin University of Science and Technology, Yulin 64002, Taiwan; Smirzaei@yuntech.edu.tw

⁴ Green intelligence Environmental School, Yangtze Normal University, Chongqing 408100, China; mvakili1981@yahoo.com

* Correspondence: gholami@ntc.zcu.cz (F.G.); Zahra.gholami@unicre.cz (Z.G.); Tel.: +420-377-634-816 (F.G.); +420-471-122-239 (Z.G.)

Received: 30 September 2020; Accepted: 11 November 2020; Published: 13 November 2020



Abstract: The catalytic performance of a series of La-Fe/AC catalysts was studied for the selective catalytic reduction (SCR) of NO by CO. With the increase in La content, the Fe²⁺/Fe³⁺ ratio and amount of surface oxygen vacancies (SOV) in the catalysts increased; thus the catalytic activity improved. Incorporating the promoters to La₃-Fe₁/active carbon (AC) catalyst could affect the catalyst activity by changing the electronic structure. The increase in Fe²⁺/Fe³⁺ ratio after the promoter addition is possibly due to the extra synergistic interaction of M (Mn and Ce) and Fe through the redox equilibrium of M³⁺ + Fe³⁺ ↔ M⁴⁺ + Fe²⁺. This phenomenon could have improved the redox cycle, enhanced the SOV formation, facilitated NO decomposition, and accelerated the CO-SCR process. The presence of O₂ enhanced the formation of the C(O) complex and improved the activation of the metal site. Mn@La₃-Fe₁/AC catalyst revealed an excellent NO conversion of 93.8% at 400 °C in the presence of 10% oxygen. The high catalytic performance of MnO_x and double exchange behavior of Mn³⁺ and Mn⁴⁺ can increase the number of SOV and improve the catalytic redox properties.

Keywords: NO reduction; CO-SCR; Mn promoter; La-Fe/AC catalyst; excess oxygen; air pollution

1. Introduction

Nitrogen oxide (NO_x) is mainly emitted from stationary and mobile combustion processes and causes many problems such as global warming, ozone depletion, photochemical smog, acid rain, visibility damage, and human health complications. Many efforts have recently been devoted to reduce and control NO_x from the air using different technologies, such as selective catalytic reduction (SCR) that converts harmful NO_x to harmless N₂. Considerable attention has been given to the development of SCR of NO_x using CO, which can efficiently remove NO and CO co-existing in many industrial exhaust gases [1–3]. However, this method has several challenges, such as resistance to O₂ and SO₂, ensuring low-temperature activation, and durable operation. The CO-SCR process shows great potential for expanded application because CO is low cost and can be simply produced without generating solid carbon deposits [4,5].

Flue gas from stationary sources has 5% higher level of oxygen than mobile exhaust gas. The CO and oxygen concentrations released from the fluidized catalytic cracking regenerators are typically in the range of 2–10 vol.% and 0.5–2 vol.%, respectively [6]. Therefore, it is crucial to develop catalysts with high activity, selectivity to N_2 , high stability, and high resistance to poisoning compounds such as SO_2 and O_2 [7]. NO_x removal with CO has been investigated. Different catalysts, such as supported Cu, Mn, and Fe-based and noble metal-supported catalysts, such as $CuO-CoO_x/\gamma-Al_2O_3$ [8], Fe-Ni [9], Mn-Cu/ZSM5 [10], $LaMn_{0.5}Cu_{0.5}O_3$ [11], Au- $CeO_x/AlTiO_x$ [12], Au/FeCe [13], Mn/ TiO_2 [14], Fe-Ba/ZSM-5 [15], and $Fe_{0.8}Co_{0.2}/ASC$ [16], have been extensively studied. Using proper support for catalysts, such as TiO_2 , Al_2O_3 , and active carbon (AC), are essential for NO_x removal by SCR at low temperatures. Their high surface areas and thermal stabilities can enhance the dispersion of the active substance of the catalyst. Carbonaceous materials with high surface area, excellent pore structure, and a low price might be an ideal support candidate for catalysts in the SCR of NO_x [17].

Iron (Fe) catalysts have a notable catalytic activity and remarkable redox capacity in $NO + CO$ reaction. Iron oxides have changeable valences, nontoxicity, low cost, good redox properties, and high oxygen storage capacities for low-temperature SCR reactions [18]. The redox-active $Fe^{3+} \leftrightarrow Fe^{2+}$ centers are responsible for the steady-state activity [9]. However, the mono iron catalyst shows weak catalytic activity for NO removal at low temperatures [19]. Chang et al. [20] and Mihai et al. [21] reported that the concentration of oxygen vacancies on the $LaFeO_3$ perovskite catalyst's surface is strongly related to the bulk oxygen concentration and the relative diffusion rate of the lattice oxygen with respect to the surface reaction. They found that the partial replacement of La with Sr at the A-site, and partial replacement of Fe with Co or Mn at the B-site of the ABO_3 perovskite, caused an increase in the surface oxygen vacancies and oxygen mobility, which can affect the catalytic activity. The introduction of A-site cation deficiency could be beneficial for adjusting the surface properties such as surface element valence state, and oxygen vacancies, and surface oxygen species; therefore, it can improve the reactivity of the catalyst [22].

The catalyst properties might be enhanced by adding promoters to form a mixed oxide catalyst, enhancing the redox properties, and improving the thermal and mechanical stability. The addition of promoter and the interaction of metal-promoter can remarkably improve the catalyst activity of metal oxide catalysts [23]. Promoters can be used as a structural, textural, electronic modifier, stabilizers, and catalyst-poison-resistant, improving the catalytic performance. Structural promoters are able to modify the surface properties by affecting the metal-support interaction, thus improving the metal dispersion and number of active metals. Different promoters, such as TiO_2 , Al_2O_3 , SiO_2 , and CeO_2 , are known as structural promoters [24]. Rare earth elements have been applied widely as an additive to Ce-based materials for CO, HC, and NO_x removal and can also act as the base sites to efficiently eliminate the coke deposition [25]. La oxides have a special surface chemical composition and physicochemical property compared with other rare earth metals. The top surface of La oxide readily undergoes carbonation and hydroxylation when exposed to air [26,27].

Among different transition metals, Mn-based catalysts have been broadly investigated due to their high potential for NO_x removal at low temperatures. Various parameters, such as morphology, surface area, crystallinity, and Mn oxidation state, affect the catalyst's activity of MnO_x . The multivalent transition metal can create several stable oxides. The activity of Mn oxides in SCR reaction is in the order of $MnO > Mn_3O_4 > Mn_2O_3 > Mn_5O_8 > MnO_2$ [28,29]. Increasing the Mn valence from Mn^{2+} to Mn^{4+} in MnO and MnO_2 , respectively, increases the number of oxygen vacancies on the catalyst's surface, thereby enhancing NO_x removal efficiency. Mn_2O_3 with high N_2 selectivity is preferred for SCR. The Mn_2O_3 activity in direct decomposition of NO and N_2O is more evident than Mn_3O_4 because of the higher oxygen lability on Mn_2O_3 than Mn_3O_4 [3,30,31].

Owing to their rich surface functional groups, high surface area, and microporous structure, carbon materials are known as important materials in many fields. They can be used as support in heterogeneous catalysts, and due to their high adsorption capacity, they can enhance the catalyst's ability to adsorb reactants for activation [32]. In this work, the catalytic activity of a series of activated

carbon-supported La-Fe (La-Fe/AC) catalysts synthesized using the co-impregnation method for NO_x removal in the presence of excess oxygen was studied, and the ratio of La to Fe was optimized to provide the highest catalytic activity. The influence of catalyst composition on the physicochemical properties and catalyst activity for the CO-SCR reaction was investigated in the presence of 10% oxygen. The promotional effect of manganese and cerium on the catalyst properties and NO_x conversion was studied. The prepared catalysts were characterized by Raman spectroscopy, X-ray diffraction (XRD), temperature-programmed desorption (CO-TPD and NO-TPD), inductively coupled plasma-optical emission spectrometry (ICP-OES), and X-ray photoelectron spectroscopy (XPS).

2. Results

2.1. Characterization of Catalysts

The molecular vibration or rotational energy and the structural disorder degree of the synthesized catalysts were studied using Raman spectroscopy. This technique is used widely for characterizing structural features of carbon materials. Figure 1, Table S1, and Figure S1 revealed that all La-Fe/AC catalysts had two peaks. A distinct peak appeared at approximately 1340 cm⁻¹ (D band) assigned to the chaos and defects of the crystalline structure of carbon material, and the peak appeared at around 1600 cm⁻¹ (G bands) assigned to the graphitic structure of carbon materials [33,34].

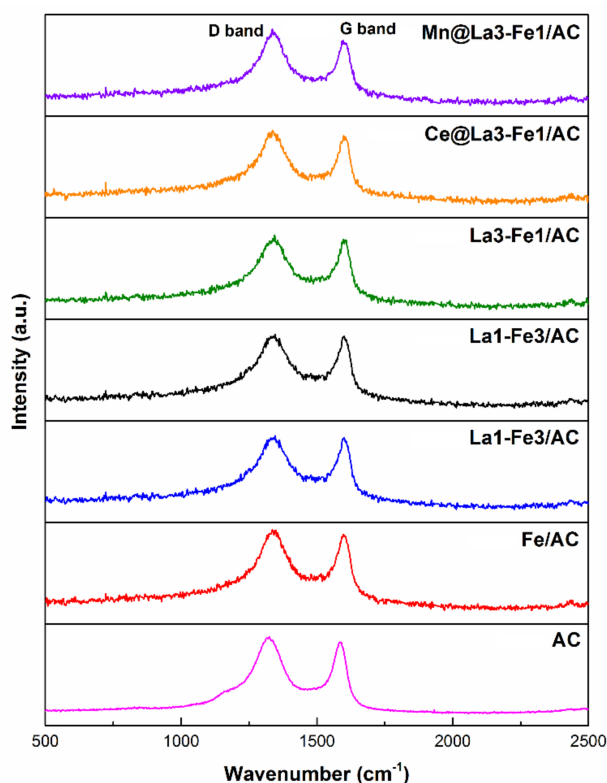


Figure 1. Raman spectroscopy of the synthesized catalysts.

The value of ID/IG was used to evaluate the degree of graphitization level, reflecting the structural proximity degree of carbon material. The lower ID/IG ratio designates a well-ordered structure of the carbon material in the catalysts. The ID/IG values of catalysts were in the following order: Mn@La₃-Fe₁/AC (2.03) > Ce@La₃-Fe₁/AC (1.70) > La₃-Fe₁/AC (1.63) > La₁-Fe₁/AC (1.51) > La₁-Fe₃/AC (1.42) > Fe/AC (0.98) > AC (0.94). There was an increase in the ID/IG ratio after loading Fe and La on AC support and reached 1.63 for the La₃-Fe₁/AC catalyst, indicating the formation of more graphitized carbon at a higher concentration of La in the catalyst structure. A further increase was observed after the addition of promoters, and the highest ID/IG was observed for the Mn@La₃-Fe₁/AC

catalyst. This result implies that the addition of promoters increased the extent of graphitization. The Mn@La3-Fe1/AC with the larger ID/IG value indicated that the catalyst's crystalline structure was slightly ruined during the preparation process compared with other catalysts.

The XRD spectra of different catalysts are shown in Figure 2. The main component of raw-activated carbon is carbon, having the main peaks with numerous clutter peaks. Two diffraction peaks attributed to AC were detected at 26° (002) and 43° (101) (JCPDS card No 41-1487). The peaks of Fe were observed in Fe/AC catalyst. The peaks at around 35° (311) and 50° (511) were assigned to Fe₃O₄ (JCPDS card No. 04-0755), and peaks at around 44.5°, 58°, and 64° were attributed to Fe₂O₃ [17,21,34–36]. The intensities of the diffraction peaks of Fe₃O₄ and Fe₂O₃ were decreased by the addition of La, Mn, and Ce, and the peaks became wider, indicating the better metal dispersion on the catalysts. Weak peaks at around 28.4°, 39.5°, and 53° were assigned to the presence of La₂O₃ in the catalysts (JCPDS card No. 05-0602). As shown in Figure 2, the intensities of the peaks for metal oxides were very weak, and also some of them were overlapped with the broad and intense carbon peaks, and the crystalline structure of iron oxides and lanthanum oxide were not clearly detected. Intensity of the peaks are proportional to the amount of the materials detected by X-ray. Due to the low amount of loaded materials in the catalyst, high dispersion, or poor crystalline state of promoter atoms, the intensity of the peaks were very weak or not observed. There are very weak peaks of Mn and Ce in XRD patterns. The weak peak corresponds to Mn₃O₄ was observed at around 18.6° in the XRD pattern of Mn@La3-Fe1/AC, and CeO₂ peaks were observed at 33.8° (200) and 56.5° (311) (JCPDS card No. 34-0394) in the XRD pattern of Ce@La3-Fe1/AC [1,4,17]. The first small peak at around 13.7° could belong to the plastic sample holder because the irradiated area of the sample was 15 × 15 mm, but the investigated powders were located only in the area of 12 × 12 mm.

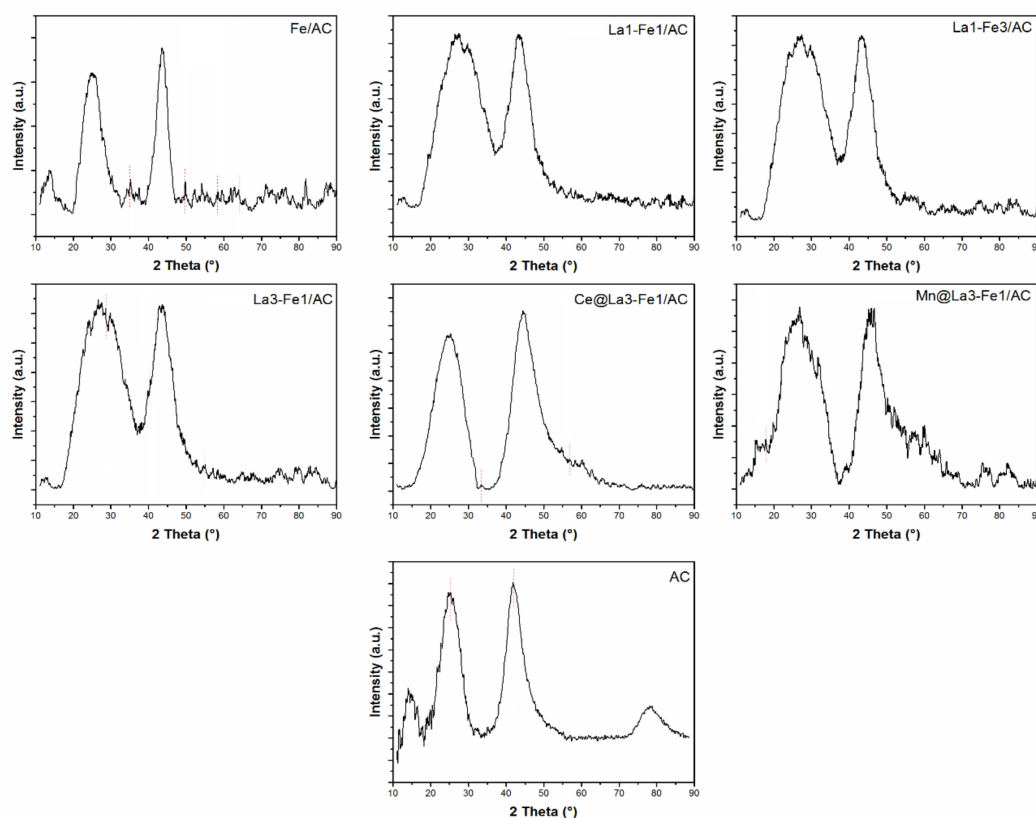


Figure 2. XRD profiles of the synthesized catalysts: Fe/AC, La1-Fe1/AC, La1-Fe3/AC, La3-Fe1/AC, Ce@La3-Fe1/AC, Mn@La3-Fe1/AC, and AC.

The XPS technique was used to analyze the composition and surface properties of La-Fe/AC. The surface elemental composition and oxidation state of the catalysts were analyzed using XPS in the

region of 0–1300 eV. The XPS survey spectrum and surface composition of the synthesized catalysts (Figure 3 and Table 1) indicated that the prepared catalysts contained Fe, La, C, O, Mn, and Ce elements. La:Fe ratios obtained from the XPS analysis were not very close to the nominal composition of the prepared catalysts. The reason could be that the XPS is highly surface selective and will reflect the composition at the surface and only a few nanometers deep down, which could be different from the elemental composition in the bulk sample. The chemical compositions of the prepared catalysts were also analyzed by inductively coupled plasma-optical emission spectrometry (ICP-OES) (Table 1). It was found that La:Fe ratios of the prepared catalysts were close to the nominal molar ratios of La and Fe for all samples.

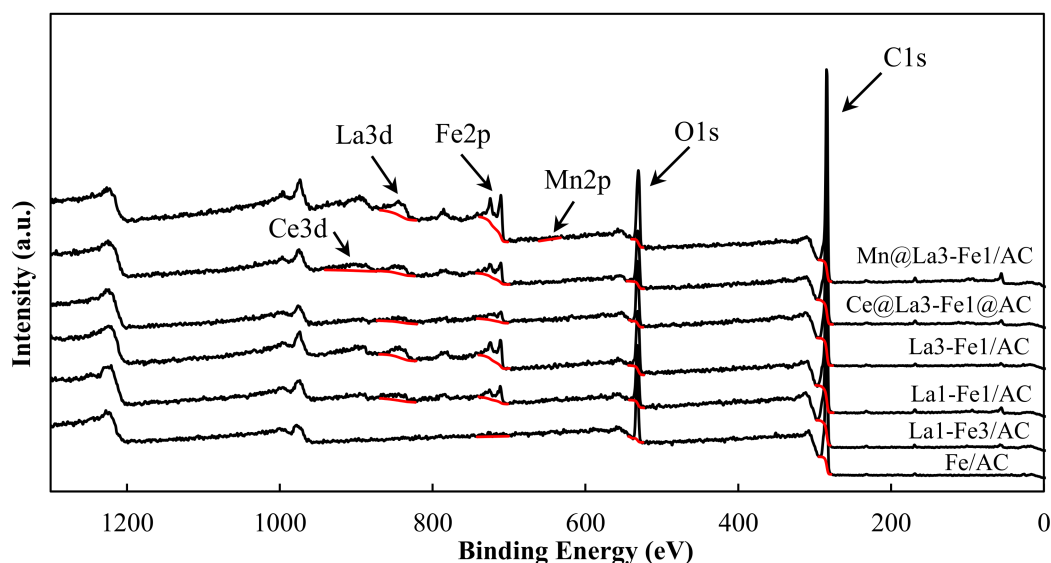


Figure 3. XPS survey spectrum of the synthesized catalysts.

Table 1. Surface composition of the synthesized catalysts.

Catalyst	Atomic Percentage (%)						^a La:Fe	^b La:Fe	^c La:Fe	^d Fe ²⁺ /Fe ³⁺
	C	O	La	Fe	Ce	Mn				
Fe/AC	85.11	13	0	1.89	0	0	0:1	0:1	0:1	0.25
La1-Fe3/AC	85.98	9.5	1.15	3.37	0	0	1:2.9	1:3.1	1:3	0.58
La1-Fe1/AC	83.15	10.28	2.42	4.15	0	0	1:1.7	1:1.2	1:1	0.72
La3-Fe1/AC	86.34	9.39	1.33	2.94	0	0	1:2.2	3:1	3:1	0.81
Ce@La3-Fe1/AC	82.46	9.75	2.18	3.97	1.64	0	1:1.8	2.8:1	3:1	1.27
Mn@La3-Fe1/AC	78.85	12.15	2.98	5.11	0	0.91	1:1.7	2.9:1	3:1	1.96

^a La:Fe ratio determined by XPS, ^b La:Fe ratio determined by ICP, ^c La:Fe ratio according to the nominal composition, ^d Area ratio of Fe²⁺/Fe³⁺ estimated by considering the deconvolution peak areas of Fe²⁺ and Fe³⁺.

Figure 4 shows the XPS spectra of Fe 2p assigned to different catalysts. The observed peaks at 711.2 and 725.5 eV were attributed to the binding energies of Fe 2p_{3/2} and Fe 2p_{1/2}, respectively. The values of 709 and 711 eV were reported for Fe²⁺ (2p_{3/2}) and Fe³⁺ (2p_{3/2}), respectively [17,35,37]. The shake-up satellite peaks at 714.02, 718.57, 731.67, and 734.40 eV correspond to Fe 2p_{3/2} and Fe 2p_{1/2} [19]. The peak at around 711.2 eV was assigned to the Fe 2p_{3/2} peaks of iron oxides, confirming that both ferrous and ferric oxides were present. Increasing the amount of La in the catalyst structure increased the ratio of Fe²⁺/Fe³⁺ (Table 1). The presence of both Fe²⁺ and Fe³⁺ was also confirmed by XRD analysis; however, due to the overlapping of the peaks for metal oxides with the wide and intense peaks of carbon materials, the crystalline structure of iron oxides were not clearly identified. The formation of Fe²⁺ might be attributable to the higher electronegativity of Fe (1.83) compared with La (1.10); therefore, Fe's tendency to capture electrons is higher than that of La. Hence, compared with La³⁺,

Fe^{3+} can easily accept the electrons to form more Fe^{2+} and resulted in a higher $\text{Fe}^{2+}/\text{Fe}^{3+}$ ratio and improved catalytic activity [38].

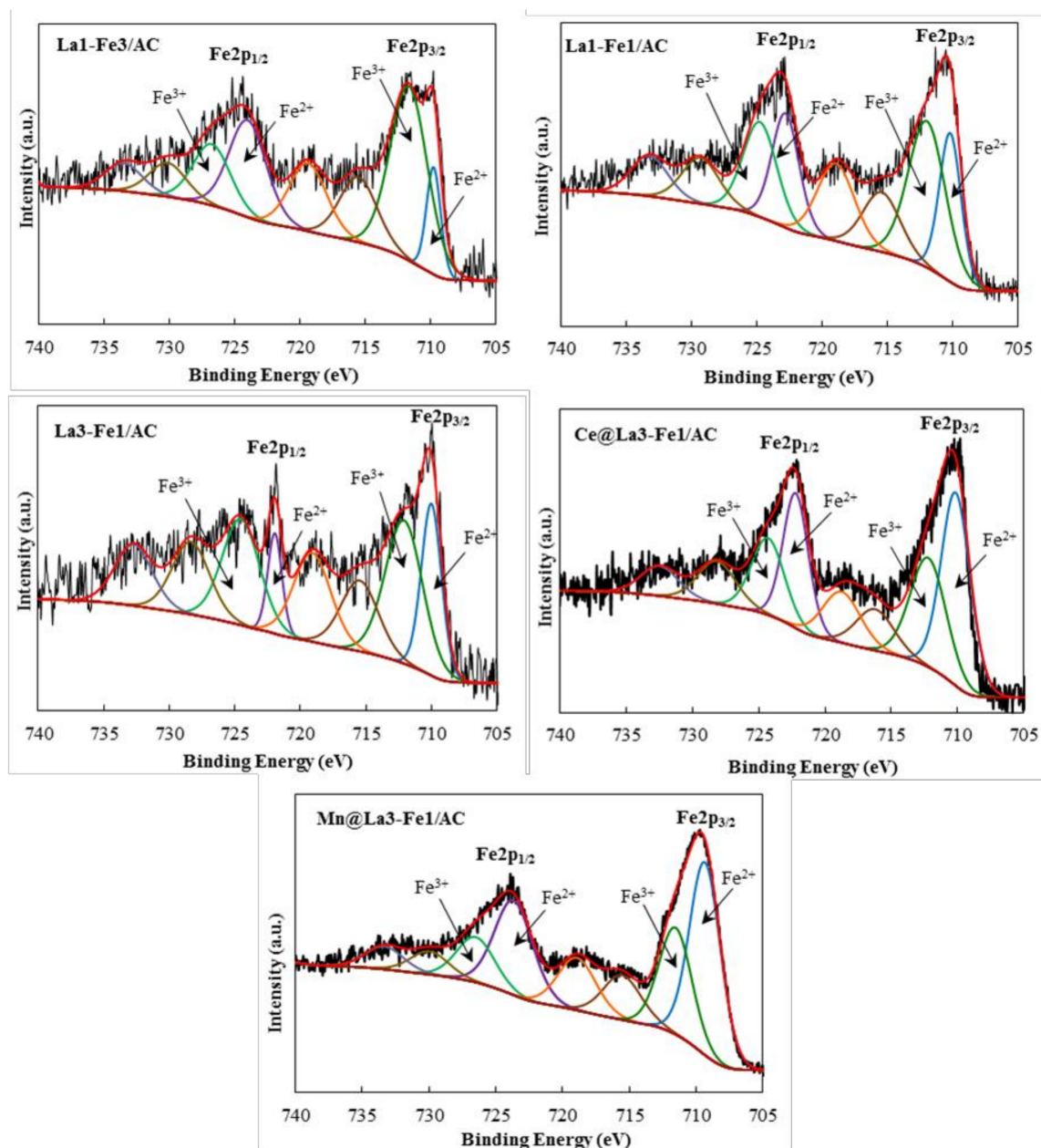


Figure 4. XPS spectrum of Fe2p of the synthesized catalysts La1-Fe3/AC, La1-Fe1/AC, La3-Fe1/AC, Ce@La3-Fe1/AC, and Mn@La3-Fe1/AC.

The redox couple ($\text{Fe}^{2+}/\text{Fe}^{3+}$) in Fe/AC catalyst indicated an electron transfer between Fe and AC supports. The catalyst activity could be affected by the incorporation of promoters, which act as a structural modifier and alter the surface properties by affecting the metal-support interaction, thus improving the metal dispersion and number of active metals and enhancing the catalyst reducibility.

XPS analysis of the catalyst (Table 1) revealed that the $\text{Fe}^{2+}/\text{Fe}^{3+}$ ratio increased by adding Ce and Mn promoters to the catalyst. Further increase in the Fe^{2+} after addition of promoter could be due to the new synergistic interaction of M (Mn or Ce) and Fe through the redox equilibrium of $\text{M}^{3+} + \text{Fe}^{3+} \leftrightarrow \text{M}^{4+} + \text{Fe}^{2+}$. The redox couples between $\text{Fe}^{2+}/\text{Fe}^{3+}$ and $\text{M}^{3+}/\text{M}^{4+}$ could improve the redox cycle, enhance the oxygen vacancies, facilitate the NO dissociation, and promote the catalytic reaction.

According to the results, the amount of Fe^{2+} species on the surface of Mn@La3-Fe1/AC catalyst was higher than other catalysts ($\text{Fe}^{2+}/\text{Fe}^{3+} = 1.96$), which resulted in enhanced catalytic activity in NO reduction by CO at low temperature.

Figure 5 and Table 2 display the XPS spectra and curve fittings of O 1s used to investigate the oxygen species on the catalysts' surface. The O 1s spectra of Fe/AC catalyst showed three different peaks. The first peak centered at 530.5 eV, ascribed to the lattice oxygen (O_β) with low binding energy related to metal-oxide (Fe–O) bond. The second peak at 531.6 eV could be ascribed to O^{2-} ions in the oxygen-deficient regions, representing the surface chemisorbed oxygen (O_α) in the matrix of catalysts. The peak at 532.9 eV could be assigned to the oxygen species in hydroxide groups and dissociated oxygen (O_γ) (O_2^- , O^{2-} , or O^- , and OH^-), respectively [20,39–43]. The O 1s peak shifted from 530.5 eV to 529.5 eV after incorporation of La to the Fe/AC catalyst. The incorporation of La into the Fe/AC catalyst increased the concentration of O_β and O_α in the La1-Fe3/AC catalyst, while O_γ oxygen species decreased on the catalyst's surface. The concentration of chemisorbed oxygen (O_α) on the catalyst surface increased from 17,665.6 to 18,171.3 by further increase in La:Fe ratio from 1:3 to 3:1. The higher concentration of chemisorbed oxygen on the surface indicated the higher oxygen vacancies on the surface of the catalysts.

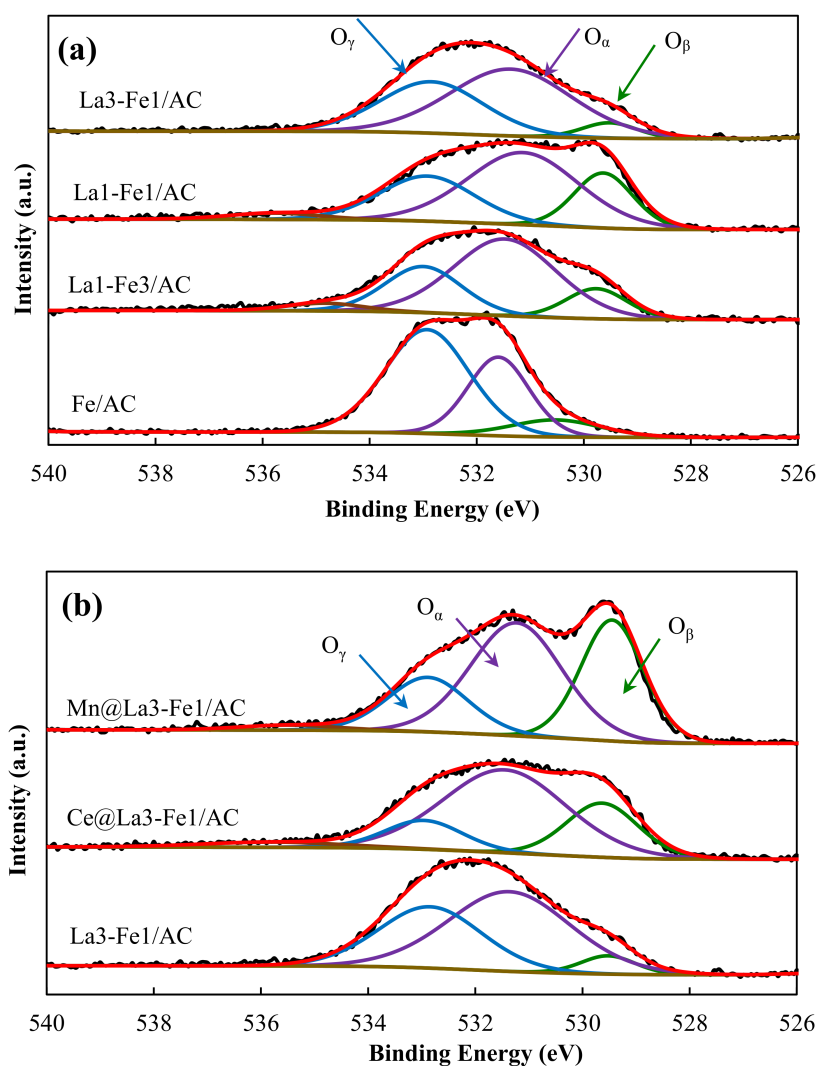


Figure 5. XPS spectrum of O 1s of the (a) La3-Fe1/AC, La1-Fe1/AC, La1-Fe3/AC, and Fe/AC, (b) Mn@La3-Fe1/AC, Ce@La3-Fe1/AC, and La3-Fe1/AC.

Table 2. Results of curve fitting of O 1s XPS spectra of the synthesized catalysts.

Catalyst	Area under the Graphs Atomic Percentage (%)		
	O _β	O _α	O _γ
Fe/AC	3426.5 10.16	10,876.4 31.99	19,496.7 57.85
La1-Fe3/AC	4090.1 13.20	17,665.6 57.04	7885.8 25.47
La1-Fe1/AC	7230.8 20.08	17,922.5 49.79	9548.5 26.54
La3-Fe1/AC	1860.4 5.84	18,171.3 57.06	11,810.6 37.10
Ce@La3-Fe1/AC	7280.4 22.88	19,004.2 59.75	4158.4 13.08
Mn@La3-Fe1/AC	14,043.9 33.05	19,341.8 45.54	8165.2 19.23

Incorporation of Ce and Mn to the La₃-Fe1/AC catalyst resulted in a further increase in the number of oxygen vacancies on the catalysts' surface and improved the catalytic activity. Incorporation of Mn increased the number of surface chemisorbed oxygen (O_α) and lattice oxygen (O_β). The surface chemisorbed oxygen with high mobility is the most active oxygen species in the SCR process. The oxygen in the gas phase can be activated by the surface chemical oxygen on the catalyst's surface, it can facilitate the oxidation of NO to NO₂ and thus accelerating the CO-SCR process [16,44–46]. Chang et al. [20] studied the surface properties of LaFeO₃ perovskite catalysts. They reported that the peak with the lowest binding energy between 527 and 531 eV was attributed to the lattice O species, whereas the chemisorbed O or OH⁻ or hydroxides species, and particularly adsorbed water species were observed at the highest binding energies between 530 and 536 eV. As shown in Figure 5, the O_α was found to be the main peak of O 1s for Mn@La₃-Fe1/AC catalyst. As it has been reported other researchers [16,47], the catalytic reaction of NO and CO could be enhanced at higher amount of O_α, which could be due to the fact that in addition to oxidizing of CO, the O_α also promote the adsorption of NO on the active sites of the catalyst. Evaluation of catalytic activity of binary Fe-Co metal oxides on semi-coke for the NO + CO reaction also revealed that the catalyst with the higher amount of O_α exhibited the highest deNO_x activity [16]. It has been proposed that this high activity was attributed to the higher amount of Brønsted acid sites, high possibility of formation oxygen vacancies, and the strong redox performance. Yao et al. [47] also reported that the catalyst with the higher surface oxygen vacancies revealed the higher activity and oxygen vacancies play an important role in NO removal by CO reaction.

The surface oxygen species is a critical factor for the NO reduction by CO, which can oxidize CO and promote the NO adsorption. The higher amount of O_α indicating the presence of more active oxygen on the surface of the catalyst. The higher oxygen vacancies, together with the higher Fe²⁺/Fe³⁺ ratio, resulted in the better catalytic performance by facilitating NO dissociation. The interaction between different species in metal oxide catalysts plays an essential role in the reduction of NO by CO. As mentioned earlier, due to the higher electronegativity of Fe, the electrons can migrate to Fe³⁺ to generate more Fe²⁺ in the catalyst, so the solid-state charge transfer redox couple on mixed-oxide catalysts (M³⁺ + Fe³⁺ ↔ M⁴⁺ + Fe²⁺) could promote the catalytic performance. The redox cycle could shift to right through varying La:Fe ratio, as well as the addition of promoters, which consequently could enhance the catalytic activity.

A critical factor for the NO reduction by CO is the catalyst ability of NO adsorption/desorption. The NO-TPD results are shown in Figure 6a. NO desorption peaks were observed at around 100–250 °C and 350–600 °C, indicating that NO was adsorbed on different active sites. The desorption peaks at lower temperatures indicating the bridge nitrates on the catalyst, and these low-temperature peaks attributed to the desorption of physically adsorbed NO from the catalysts' surface. The peaks at higher temperatures (350–600 °C) indicating the presence of a large number of NO_x species (nitrates and nitrites), with high thermostability on the surface, which could be decomposed at high temperatures [9,48,49].

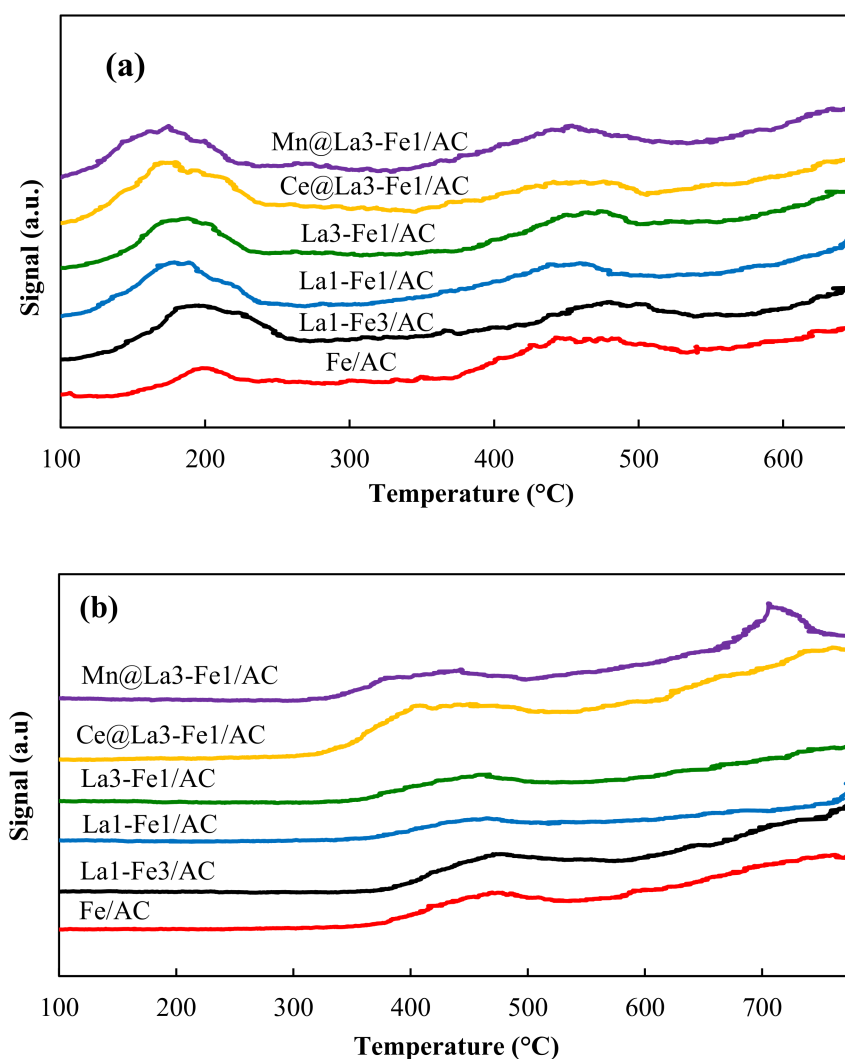


Figure 6. (a) NO-TPD and (b) CO-TPD profiles of the synthesized catalysts.

The amount of desorbed NO from the surface of catalysts was approximately compared based on the areas under the NO-TPD graphs. The amount of desorbed gas was almost doubled by the addition of La to Fe/AC catalyst, but it was not changed too much for the other catalysts. The total amount of desorbed NO from the surface of the catalysts is in this order: Fe/AC (642) < La₃-Fe₁/AC (1276) < La₁-Fe₃/AC ≈ La₁-Fe₁/AC ≈ Ce@La₃-Fe₁/AC (~1330–1340) < Mn@La₃-Fe₁/AC (1364). Compared with the Fe/AC catalyst, more bridged nitrates on the surface of the La-Fe/AC catalyst could participate in the lower temperature NO + CO reaction. Thus, it can be concluded that the higher amount of NO could be adsorbed and dissociated at lower temperatures using the catalysts with a higher La amount, which consequently resulted in higher catalytic activity. The addition of Ce and Mn promoters influenced the NO desorption behavior of the samples, and desorption peaks were shifted to lower temperatures. The Mn@La₃-Fe₁/AC catalyst may have more unpaired electrons among other samples. The weakening of the N–O bonds occur due to back-donation and releasing of the unpaired electrons into the empty antibonding orbital of the adsorbed NO species, leading to dissociation of adsorbed NO species. These Mn species may interact strongly with the surface cations and result in an increased number of defects and more active oxygen species such as Mn⁴⁺–O–Fe³⁺ on the surfaces. The Mn⁴⁺–O–Fe³⁺ oxygen species could be easily reduced to Mn³⁺–□–Fe²⁺, resulting in excellent catalytic efficiency.

The surface oxygen vacancy (SOV) is an important parameter to weaken the N–O band, dissociating NO to produce O and N radicals. During the NO + CO reaction, first, the active

metals on the catalyst surface were reacted with CO to generate SOVs on the surface of catalysts. Then, the NO molecules were activated by the SOVs to produce N and O radicals. The O radicals were reacting with adsorbed CO molecules on Fe^{2+} species to produce CO_2 , and N radicals could be combined with another NO molecule to make N_2O or combined with another N radical to produce N_2 . N_2O can be considered as the intermediate for NO reduction into N_2 . These findings are in good accordance with the results reported by Shi et al. [19], who studied the Mn-modified copper and iron catalysts and investigated their catalytic activity for NO reduction by CO. It was found that the Mn^{4+} on the surface of the catalyst can generate reactive oxygen species, which can be more easily reduced to create some oxygen vacancies during the reaction.

The CO-TPD analysis was performed to study the CO adsorption behavior on the catalyst's surface (Figure 6b). As shown in CO-TPD profiles, two peaks appeared at around 350–550 °C and 600–750 °C, indicating the presence of different types of activated adsorption sites with different binding strengths on the surface of the catalysts. CO was difficult to desorb from Fe/AC at low temperatures. The lanthanum addition to the catalyst affected the CO desorption behavior, and desorption peaks shifted to lower temperatures. According to the areas under the CO-TPD graphs, the amount of desorbed CO from the surface of the catalyst increased by the addition of La to Fe/AC. The peaks were growing and shifting to the lower temperatures by adding Ce and Mn into the catalyst; thus, the CO adsorption capacity increased. It is believed that the Fe^{2+} species on the catalyst's surface are the active sites for CO adsorption. The higher temperature of adsorption and desorption of CO for Fe/AC catalyst, together with a lower amount of Fe^{2+} , can result in the low catalytic activity in NO reduction by CO. Presence of the desorption peaks at lower temperatures for the promoted catalysts attributed to the rich Fe^{2+} species on the catalyst's surface, which was also confirmed by the XPS analysis (Table 1). According to the areas under the CO-TPD graphs, the total amount of desorbed gas is following the order: $\text{Mn@La}_3\text{-Fe}_1/\text{AC}$ (1809) > $\text{Ce@La}_3\text{-Fe}_1/\text{AC}$ (1612) > $\text{La}_1\text{-Fe}_3/\text{AC}$ (1014) > $\text{La}_3\text{-Fe}_1/\text{AC}$ (577) > $\text{La}_1\text{-Fe}_1/\text{AC}$ (385) > Fe/AC (338). Among these catalysts, the $\text{Mn@La}_3\text{-Fe}_1/\text{AC}$ exhibited the lowest desorption temperature, which could be ascribed to the higher content of Fe^{2+} on the catalyst surface, resulting in the slightly higher catalytic activity in the NO + CO reaction.

2.2. Catalytic Activity Evaluation

The catalytic activity can be influenced by catalyst nature and its structure, such as uniform dispersion of metal species, high surface area, and mesoporous structure. Figure 7a shows that the maximum NO conversion of 64.4% was obtained for Fe/AC at 400 °C. The addition of transition metal oxides into the catalyst can improve the redox properties and thermal stability of the composite materials. It has been reported that the carbon-based materials loaded with transition metals reveal high activity in NO_x reduction by CO [16,50]. The physicochemical properties of the catalyst can affect the catalytic pathway [51,52]. The addition of La can be beneficial for NO conversion into N_2 and further enhancement of the catalytic activity [53,54]. The lanthanum with the electronic structure of $4f^0 5d^1 6s^2$ has only one electron in 5d orbital and can provide proper electron transfer orbital. The rare earth elements compounds have high catalytic activity and can be used as catalysts for the electron transfer station [55]. Increasing the amount of La enhanced the NO conversion at the temperature range between 200–400 °C. Figure 7a shows that the $\text{La}_3\text{-Fe}_1/\text{AC}$ catalyst with a higher content of La showed the highest NO_x conversion compared with other catalysts. As it was mentioned earlier, the characterization results revealed that the variation of La:Fe ratio in the catalysts resulted in different interactions between La and Fe, which affects the formation of Fe^{2+} and Fe^{3+} species, whereas the $\text{Fe}^{2+}/\text{Fe}^{3+}$ ratio increased from 0.58 for $\text{La}_1\text{-Fe}_3/\text{AC}$ to 0.81 for $\text{La}_3\text{-Fe}_1/\text{AC}$. The higher $\text{Fe}^{2+}/\text{Fe}^{3+}$ ratio enhanced the CO adsorption and NO dissociation and resulted in higher catalytic activity. The large gradient of electronegativity between La (1.10) and Fe (1.83) is useful for shifting the redox equilibrium to the right and generating more Fe^{2+} species on the surface of the catalyst.

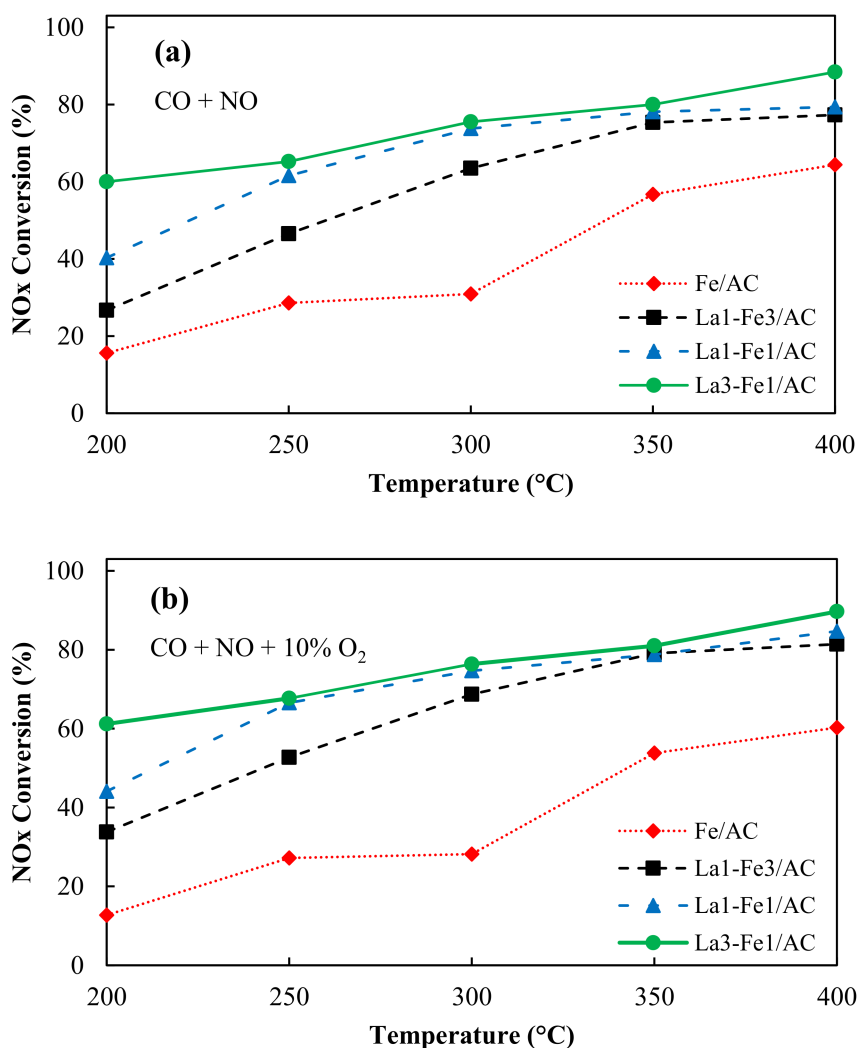
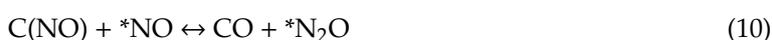
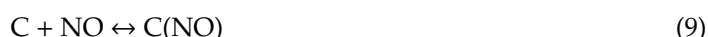


Figure 7. NO_x conversion over La-Fe/AC catalysts (a) in the absence of oxygen and (b) in the presence of oxygen, reaction conditions: NO = 250 ppm, CO = 5000 ppm, total flow rate: 350 mL/min; temperature: 200–400 °C, catalyst: 200 mg, GHSV = 26,000 h⁻¹.

During the catalyst preparation via the co-impregnation method, the low-valence-state Fe species and additional oxygen vacancies were created, enhancing the adsorption of CO and dissociation of NO species and improve the catalytic activity. The obtained results for the catalyst activity tests were in good consistent with the XPS and TPD results. The activity test revealed that the Mn@La₃-Fe1/AC catalyst with the highest Fe²⁺/Fe³⁺ ratio (obtained from XPS analysis) has the highest activity. NO reduction by CO was enhanced by the synergistic effect of SOV and Fe²⁺ species.

In the absence of oxygen and 400 °C, the NO_x conversions of 77.3%, 79.4%, and 88.4% for La1-Fe3/AC, La1-Fe1/AC, and La3-Fe1/AC were obtained, respectively (Figure 7a). Ramana et al. [27] found that the changes in the surface chemical composition and structural properties of La₂O₃ led to improved catalytic activity and stability of the catalysts. Lanthanum nitrate (La[NO₃]₃) was converted to La₂O₃ after calcination and improved the NO_x conversion.

In the presence of 10% O₂ at 400 °C, the NO_x conversion increased slightly to 60.3%, 81.4%, 84.7%, and 89.7% for Fe/AC, La1-Fe3/AC, La1-Fe1/AC, and La3-Fe1/AC, respectively (Figure 7b). The O₂ was adsorbed into the carbon site of the support to form C(O) complex. The reaction of C(O) with an oxidized metal site (*O) that formed CO₂ and activated the metal site (*) can be used later for the reduction of NO to N₂O or N₂. The mechanism can be expressed as the following reactions [56]:



According to this reaction mechanism, the presence of the metal site is crucial for the gasification of carbon and the reaction of NO and carbon sites. The presence of O₂ in the flue gas can enhance the creation of a C(O) complex and improve the activation of the metal site (*). O₂ can significantly affect the NO reduction by carbon because of the enhancement effect of surface oxygen complex. More than 80% of NO conversion was obtained at 400 °C in the presence of 10% O₂. The roles of carbon sites, oxygen, and metal sites in the NO reduction are exhibited in reactions 1, 2, 3, 9, and 10.

It is worth mentioning that a negligible amount of NO₂ (less than 5 ppm) was detected for all catalysts in the presence of oxygen during the reaction. Actually, by the addition of oxygen to the feed gas, about 10–50 ppm NO₂ was formed due to the fast homogeneous gas-phase oxidation of NO to NO₂ (NO + O₂ → 2 NO₂); and after about 2 min of reaction, NO₂ concentration was significantly decreased to less than 5 ppm, remained almost constant till the end of the reaction. Then, the formed NO₂ reacted with CO and produce N₂ (2 NO₂ + 4 CO → N₂ + 4 CO₂) [57]. The NO₂ formation during the reaction in the absence of oxygen was also negligible during 6 h of reaction (less than 5 ppm). The NO_x conversion of 90.4% was achieved at 400 °C for the Ce@La₃-Fe1/AC catalyst (Figure 8a). The addition of Ce as a promoter to the catalyst can enhance the low-temperature activity of the catalyst and the ability for NO_x reduction and also increase the catalyst stability [58,59].

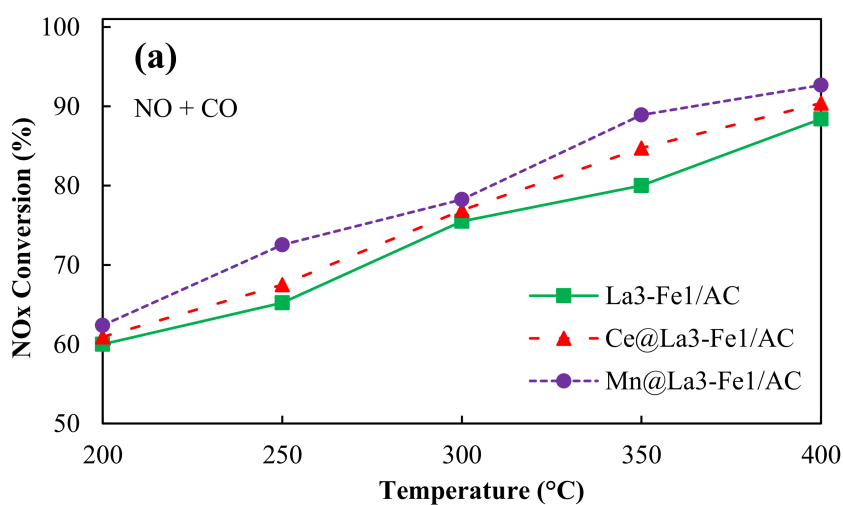


Figure 8. Cont.

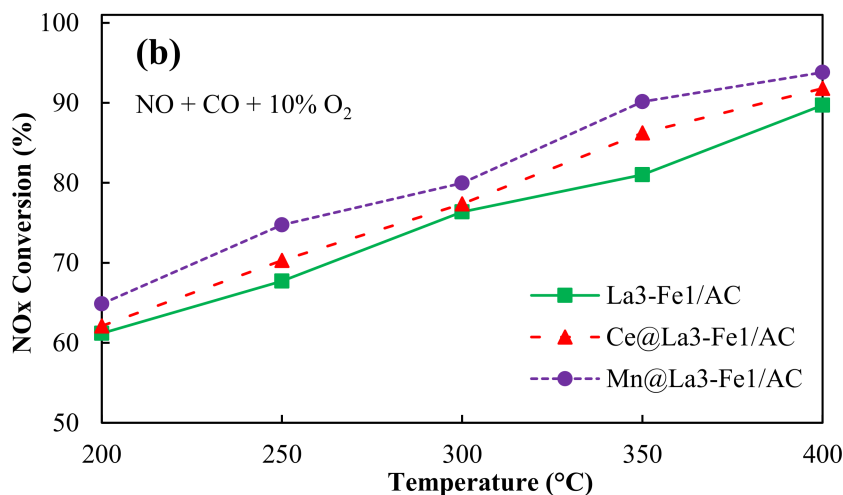


Figure 8. NO_x conversion over promoted La₃-Fe₁/AC catalysts (a) in the absence of oxygen and (b) in the presence of oxygen, reaction conditions: NO = 250 ppm, CO = 5000 ppm, total flow rate: 350 mL/min; Temperature: 200–400 °C, catalyst: 200 mg, GHSV = 26,000 h⁻¹.

Oxygen can be absorbed by Ce in reductive conditions and released in oxidative conditions for oxidation because of reversible conversion between electronic states Ce³⁺ and Ce⁴⁺. It has been reported that the incorporation of Ce⁴⁺ into the lattice of La³⁺ resulted in the formation of solid solution and increased the catalyst resistance against sintering at high temperatures, which stabilized the active metals [60]. The maximum NO_x conversion of 92.7% was obtained for Mn@La₃-Fe₁/AC catalyst in the absence of oxygen at 400 °C because of the high catalytic performance of MnO_x (Figure 8a). In comparison with other metals, manganese (Mn) is a less toxic component that can be used as a catalyst for the SCR of NO [61]. Chen et al. [17] reported that the modification of Fe₂O₃/AC catalysts with Mn species resulted in a high dispersion of manganese and iron oxides over the AC support, a larger surface area, higher amounts of Mn⁴⁺/Mn³⁺, and stronger reduction ability, which caused an enhancement in the SCR performance of the catalyst. The presence of O₂ resulted in a slight enhancement in the NO_x conversion of the catalyst by increasing the surface oxygen complex. Thus, Figure 8b shows the NO_x conversion of Ce@La₃-Fe₁/AC and Mn@La₃-Fe₁/AC enhanced to 91.8% and 93.8%, respectively, in the presence of 10% O₂.

Figures 7 and 8 show that the NO_x conversion over the La-Fe/AC catalyst was enhanced by increasing the temperature from 200 °C to 400 °C. The elevation of the temperature could result in increasing the SOV formation. Increasing the reaction temperature can provide adequate energy for dissociation of NO on SOV. Additionally, Fe²⁺ can adsorb the CO molecules during CO oxidation, thereby resulting in an improved reaction. The chemisorption of CO on active metal sites and increased SOV on the catalyst's surface resulted in the enhanced catalytic performance in the CO-SCR reaction.

3. Materials and Methods

3.1. Catalyst Preparation

A commercial activated carbon (Sigma-Aldrich, Prague, Czech Republic) was used as a support material. The AC was pretreated by soaking in the acid mixture of HNO₃ and H₂SO₄ (HNO₃:H₂SO₄ ratio of 3:1 [v/v]) for 24 h at room temperature with gentle shaking. The samples were then filtered and washed with deionized water. Then, the AC was dried at 110 °C for 24 h. The catalysts supported on AC with different molar ratios of La:Fe (i.e., 0:1, 1:1, 1:0, 1:3, and 3:1) with the total metal loading of 20 wt.% were prepared using the co-impregnation method. The proper amounts of precursors of Fe(NO₃)₃·9·H₂O (99.999%, Sigma-Aldrich, Prague, Czech Republic) and La(NO₃)₃·6·H₂O (98%, Sigma-Aldrich, Prague, Czech Republic) were dissolved in deionized water and added dropwise to the AC support with constant stirring for 6 h. The obtained impregnates then dried at 120 °C for 12 h

followed by the thermal treatment at 400 °C for 3 h under N₂ atmosphere. The 5 wt.% of Mn and Ce-promoted La-Fe/AC catalyst were synthesized by the same method using the nitrate salts of the precursors, Mn(NO₃)₂·4 H₂O (97.5%, Acros Organics, Prague, Czech Republic) and Ce(NO₃)₃·6 H₂O (99% Sigma-Aldrich, Prague, Czech Republic).

3.2. Catalyst Characterization

The X-ray diffractometer with Cu K α radiation ($k = 1.5408 \text{ \AA}$) at 60 kV and 80 mA (XRD, D8 ADVANCE Rigaku D/max-RB, Tokyo, Japan) was used to study the phase structure of the catalysts. The Raman analysis for the samples was performed using DXR Raman Microscopy, using backscattering geometry with a Nd:YVO₄ DPSS (532 nm) laser source. The spectra were recorded in the range of 500–2500 cm⁻¹ with a spectral resolution of 1 cm⁻¹. X-ray photoelectron spectroscopy (XPS) spectra of the samples were obtained using the Thermo Scientific K-alpha photoelectron spectrometer (Waltham, MA, USA). The Thermo Scientific™ Avantage Software was used for XPS data processing. Inductively coupled plasma-optical emission spectrometer (ICP-OES, Agilent 725, Agilent Technologies Inc., Santa Clara, CA, USA) was used to determine the catalysts' composition, after the total digestion of the sample in aqua regia. The temperature program desorption (TPD) of NO and CO analysis were performed through a flow reactor equipped with a thermal conductivity detector (TCD). The requisite amount of catalyst was heated from room temperature to 300 °C (10 °C/min), held for 60 min in helium flow of 30 mL/min, and then cooled down to room temperature. The sample was then exposed to 5 vol.% NO/He for NO-TPD and 10 vol.% CO/He for CO-TPD for 30 min. Afterward, helium was purged for 30 min to eliminate the physically adsorbed CO and NO from the surface of the sample. The sample was then heated to 600 °C (CO-TPD) and 800 °C (NO-TPD) in helium flow with a rate of 10 °C/min. The TCD was used to monitor the consumption of NO and CO during the analysis. Mettler Toledo thermal analysis system was used to measure weight changes of the sample when heated under a flow of nitrogen and also air at a constant heating rate of 10 °C/min from 25 °C to 900 °C.

3.3. Catalyst Activity Test

The catalyst activity was measured in a fixed-bed tubular reactor at atmospheric pressure using 400 mg of catalyst powder at a temperature range between 200 °C to 400 °C. Figure 9 shows the schematic of the experimental setup. The stainless steel K-Type thermocouple temperature sensor was located inside the reactor tube, near the catalyst bed. The catalyst was flushed in-situ with helium at 200 °C for 1 h before the activity measurement. The furnace temperature was adjusted to the required reaction temperature, and the reactor was supplied with the reactant gas mixture with a composition of 250 ppm NO, 0%–10% O₂, and 5000 ppm CO in He. The total flow rate of the feed gas was 350 mL/min with the gas hourly space velocity (GHSV) of 26,000 h⁻¹. The concentration of NO and CO in feed gas was determined according to the industrial flue gas, which contains 100–1000 ppm NO and 2000–50,000 ppm CO, respectively. The composition of the outlet gas (including NO, NO₂, NO_x) during 6 h of reaction was analyzed using a chemiluminescence analyzer (CAI-600 HCLD, California Analytical Instruments, CA, USA). The NO_x conversion was calculated using the following equation:

$$x\% = \frac{C_{NO_x,in} - C_{NO_x,out}}{C_{NO_x,in}} \times 100 \quad (11)$$

where $C_{NO_x,in}$ is the initial concentration of NO_x, and $C_{NO_x,out}$ is the concentration of NO_x in the outlet gas.

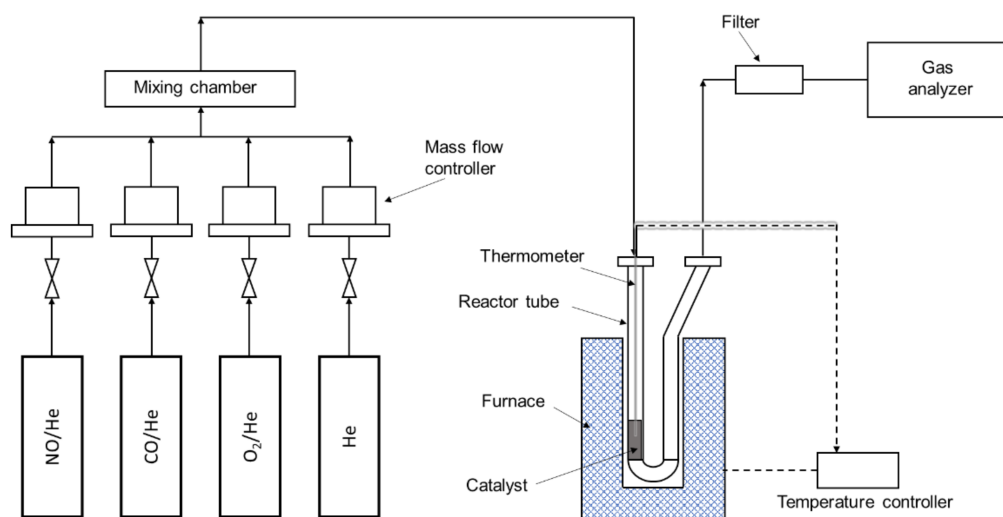


Figure 9. Schematic of the fixed-bed tubular reactor for the CO-SCR reaction.

4. Conclusions

The reduction of NO_x by CO offers a simple and low-cost technology for reducing NO_x emissions from mobile or stationary sources. In this study, NO_x removal by CO was investigated over a series of La-Fe catalysts supported on activated carbon synthesized using co-impregnation. Based on the above experiments, the paper mainly draws the following conclusions:

La-containing catalysts showed enhanced NO conversion compared to Fe/AC catalyst. Introducing La into the catalysts increased the $\text{Fe}^{2+}/\text{Fe}^{3+}$ ratio, and SOV in the catalysts, thereby improving the catalytic activity. Incorporation of Ce and Mn also increased the number of oxygen vacancies and lattice oxygen and facilitated the oxidation of NO to NO_2 , and so accelerated the CO-SCR process. The synergistic interaction of promoter agent (Mn and Ce) and Fe through the redox equilibrium of $\text{M}^{3+} + \text{Fe}^{3+} \leftrightarrow \text{M}^{4+} + \text{Fe}^{2+}$ resulted in a further increase in the amount of Fe^{2+} . The redox couples may have improved the redox cycle and consequently enhanced the formation of oxygen vacancies, facilitated NO decomposition, and promoted the catalytic reaction. The Mn-modified catalyst with better dispersion of the amorphous state, high amounts of $\text{Fe}^{2+}/\text{Fe}^{3+}$ and $\text{Mn}^{4+}/\text{Mn}^{3+}$, and SOV amount showed the highest catalytic activity. The increased number of SOV can improve the catalyst's redox properties because of the double exchange behavior of Mn^{3+} and Mn^{4+} . The NO_x conversion of 92.7% was obtained over Mn@La3-Fe1/AC catalyst in the absence of oxygen at 400 °C; this catalyst also exhibited NO_x conversion of 93.8% in the presence of 10% oxygen and at 400 °C.

In future work, the effects of reductive pretreatments and different promoters' concentrations on the performance of catalysts will be investigated. Additional analyses to find the most available oxygen atoms and the maximum reducibility of the catalysts could be beneficial for evaluating the physicochemical properties of the catalysts.

Supplementary Materials: The following are available online at <http://www.mdpi.com/2073-4344/10/11/1322/s1>, Figure S1: Raman spectroscopy of the prepared catalysts, Figure S2: XPS spectrum of La3d, Ce3d and Mn2p of the La-Fe/AC catalysts, Figure S3: TGA analysis for AC, under air and nitrogen, Table S1: Raman Spectroscopy analysis for the prepare catalysts, Table S2: Details for the peak deconvolution XPS spectrum of the prepared catalysts.

Author Contributions: Conceptualization and experimental work designed and supported by F.G. and Z.G.; the characterizations, catalyst evaluation, and analysis were done by F.G., Z.G., M.T., V.V., S.M. and M.V.; the manuscript was written and amended by F.G. and Z.G. All authors have read and agreed to the published version of the manuscript.

Funding: This publication is a result of the project CATAMARAN, Reg. No. CZ.02.1.01/0.0/0.0/16_013/0001801, which has been co-financed by European Union from the European Regional Development Fund through the Operational Programme Research, Development and Education. This project has also been financially supported by the Ministry of Industry and Trade of the Czech Republic which has been providing institutional support for

long-term conceptual development of research organisation. The project CATAMARAN has been integrated into the National Sustainability Programme I of the Ministry of Education, Youth and Sports of the Czech Republic (MEYS) through the project Development of the UniCRE Centre (LO1606). The result was achieved using the infrastructure of the project Efficient Use of Energy Resources Using Catalytic Processes (LM2018119) which has been financially supported by MEYS within the targeted support of large infrastructures. The result was also developed within the CENTEM project, reg. no. CZ.1.05/2.1.00/03.0088, cofunded by the ERDF as part of the Ministry of Education, Youth and Sports OP RDI programme and, in the follow-up sustainability stage, supported through CENTEM PLUS (LO1402) by financial means from the Ministry of Education, Youth and Sports under the “National Sustainability Programme I”.

Conflicts of Interest: The authors declare no conflict of interest. The funders had no role in the design of the study; in the collection, analyses, or interpretation of data; in the writing of the manuscript, or in the decision to publish the results.

References

1. Gholami, Z.; Luo, G. Low-Temperature Selective Catalytic Reduction of NO by CO in the Presence of O₂ over Cu:Ce Catalysts Supported by Multiwalled Carbon Nanotubes. *Ind. Eng. Chem. Res.* **2018**, *57*, 8871–8883. [[CrossRef](#)]
2. Gholami, Z.; Luo, G.; Gholami, F. The influence of support composition on the activity of Cu:Ce catalysts for selective catalytic reduction of NO by CO in the presence of excess oxygen. *New J. Chem.* **2020**, *44*, 709–718. [[CrossRef](#)]
3. Gholami, F.; Tomas, M.; Gholami, Z.; Vakili, M. Technologies for the nitrogen oxides reduction from flue gas: A review. *Sci. Total. Environ.* **2020**, *714*, 136712. [[CrossRef](#)] [[PubMed](#)]
4. Bahrami, S.; Niaei, A.; Illán-Gómez, M.J.; Tarjomannejad, A.; Mousavi, S.M.; Albaladejo-Fuentes, V. Catalytic reduction of NO by CO over CeO₂-MO_x (0.25) (M = Mn, Fe and Cu) mixed oxides—Modeling and optimization of catalyst preparation by hybrid ANN-GA. *J. Environ. Chem. Eng.* **2017**, *5*, 4937–4947. [[CrossRef](#)]
5. Dai, X.; Jiang, W.; Wang, W.; Weng, X.L.; Shang, Y.; Xue, Y.; Wu, Z. Supercritical water syntheses of transition metal-doped CeO₂ nano-catalysts for selective catalytic reduction of NO by CO: An in situ diffuse reflectance Fourier transform infrared spectroscopy study. *Chin. J. Catal.* **2018**, *39*, 728–735. [[CrossRef](#)]
6. Li, J.; Luo, G.; Chu, Y.; Wei, F. Experimental and modeling analysis of NO reduction by CO for a FCC regeneration process. *Chem. Eng. J.* **2012**, *184*, 168–175. [[CrossRef](#)]
7. Sierra-Pereira, C.A.; Urquieta-González, E.A. Reduction of NO with CO on CuO or Fe₂O₃ catalysts supported on TiO₂ in the presence of O₂, SO₂ and water steam. *Fuel* **2014**, *118*, 137–147. [[CrossRef](#)]
8. Zhang, L.; Yao, X.; Lu, Y.; Sun, C.; Tang, C.; Gao, F.; Dong, L. Effect of precursors on the structure and activity of CuO-CoOx/γ-Al₂O₃ catalysts for NO reduction by CO. *J. Colloid Interface Sci.* **2018**, *509*, 334–345. [[CrossRef](#)]
9. Du, X.; Yao, T.-L.; Wei, Q.; Zhang, H.; Huang, Y. Investigation of Fe-Ni Mixed-Oxide Catalysts for the Reduction of NO by CO: Physicochemical Properties and Catalytic Performance. *Chem. Asian J.* **2019**, *14*, 2966–2978. [[CrossRef](#)]
10. Wang, T.; Zhang, X.; Liu, J.; Liu, H.; Wang, Y.; Sun, B. Effects of temperature on NO_x removal with Mn-Cu/ZSM5 catalysts assisted by plasma. *Appl. Therm. Eng.* **2018**, *130*, 1224–1232. [[CrossRef](#)]
11. Tarjomannejad, A.; Farzi, A.; Niaei, A.; Salari, D. NO reduction by CO over LaB_{0.5}B′_{0.5}O₃ (B = Fe, Mn, B′ = Fe, Mn, Co, Cu) perovskite catalysts, an experimental and kinetic study. *J. Taiwan Inst. Chem. Eng.* **2017**, *78*, 200–211. [[CrossRef](#)]
12. Wang, X.; Wu, X.; Maeda, N.; Baiker, A. Striking activity enhancement of gold supported on Al-Ti mixed oxide by promotion with ceria in the reduction of NO with CO. *Appl. Catal. B Environ.* **2017**, *209*, 62–68. [[CrossRef](#)]
13. Ilieva, L.; Pantaleo, G.; Velinov, N.; Tabakova, T.; Petrova, P.; Ivanov, I.; Avdeev, G.; Paneva, D.; Venezia, A. NO reduction by CO over gold catalysts supported on Fe-loaded ceria. *Appl. Catal. B Environ.* **2015**, *174*, 176–184. [[CrossRef](#)]
14. Boningari, T.; Pavani, S.M.; Ettireddy, P.R.; Chuang, S.S.; Smirniotis, P.G. Mechanistic investigations on NO reduction with CO over Mn/TiO₂ catalyst at low temperatures. *Mol. Catal.* **2018**, *451*, 33–42. [[CrossRef](#)]
15. Zhang, X.; Ma, C.; Cheng, X.; Wang, Z. Performance of Fe-Ba/ZSM-5 catalysts in NO + O₂ adsorption and NO + CO reduction. *Int. J. Hydrogen Energy* **2017**, *42*, 7077–7088. [[CrossRef](#)]

16. Wang, L.; Cheng, X.; Wang, Z.; Ma, C.; Qin, Y. Investigation on Fe-Co binary metal oxides supported on activated semi-coke for NO reduction by CO. *Appl. Catal. B Environ.* **2017**, *201*, 636–651. [[CrossRef](#)]
17. Chen, J.; Zhu, B.; Sun, Y.; Yin, S.; Zhu, Z.; Li, J. Investigation of Low-Temperature Selective Catalytic Reduction of NO_x with Ammonia over Mn-Modified Fe₂O₃/AC Catalysts. *J. Braz. Chem. Soc.* **2017**, *29*, 79–87. [[CrossRef](#)]
18. Xiong, Z.-B.; Wu, C.; Hu, Q.; Wang, Y.-Z.; Jin, J.; Lu, C.-M.; Guo, D.-X. Promotional effect of microwave hydrothermal treatment on the low-temperature NH₃-SCR activity over iron-based catalyst. *Chem. Eng. J.* **2016**, *286*, 459–466. [[CrossRef](#)]
19. Shi, X.; Chu, B.; Wang, F.; Wei, X.; Teng, L.; Fan, M.; Li, B.; Dong, L.; Dong, L. Mn-Modified CuO, CuFe₂O₄, and γ-Fe₂O₃ Three-Phase Strong Synergistic Coexistence Catalyst System for NO Reduction by CO with a Wider Active Window. *ACS Appl. Mater. Interfaces* **2018**, *10*, 40509–40522. [[CrossRef](#)]
20. Chang, H.; Bjørgum, E.; Mihai, O.; Yang, J.; Lein, H.L.; Grande, T.; Raaen, S.; Zhu, Y.-A.; Holmen, A.; Chen, D. Effects of Oxygen Mobility in La-Fe-Based Perovskites on the Catalytic Activity and Selectivity of Methane Oxidation. *ACS Catal.* **2020**, *10*, 3707–3719. [[CrossRef](#)]
21. Mihai, O.; Chen, D.; Holmen, A. Chemical looping methane partial oxidation: The effect of the crystal size and O content of LaFeO₃. *J. Catal.* **2012**, *293*, 175–185. [[CrossRef](#)]
22. Wu, M.; Chen, S.; Xiang, W. Oxygen vacancy induced performance enhancement of toluene catalytic oxidation using LaFeO₃ perovskite oxides. *Chem. Eng. J.* **2020**, *387*, 124101. [[CrossRef](#)]
23. Gholami, Z.; Luo, G.; Gholami, F.; Yang, F. Recent advances in selective catalytic reduction of NO_x by carbon monoxide for flue gas cleaning process: A review. *Catal. Rev.* **2020**, 1–52. [[CrossRef](#)]
24. Gholami, Z.; Tišler, Z.; Rubáš, V. Recent advances in Fischer-Tropsch synthesis using cobalt-based catalysts: A review on supports, promoters, and reactors. *Catal. Rev.* **2020**, 1–84. [[CrossRef](#)]
25. Lu, J.; Li, X.; He, S.; Han, C.; Wan, G.; Lei, Y.; Chen, R.; Liu, P.; Chen, K.; Zhang, L.; et al. Hydrogen production via methanol steam reforming over Ni-based catalysts: Influences of Lanthanum (La) addition and supports. *Int. J. Hydrogen Energy* **2017**, *42*, 3647–3657. [[CrossRef](#)]
26. Lu, J.; Hao, H.; Zhang, L.; Xu, Z.; Zhong, L.; Zhao, Y.; He, D.; Liu, J.; Chen, D.; Pu, H.; et al. The investigation of the role of basic lanthanum (La) species on the improvement of catalytic activity and stability of HZSM-5 material for eliminating methanethiol-(CH₃SH). *Appl. Catal. B Environ.* **2018**, *237*, 185–197. [[CrossRef](#)]
27. Ramana, C.V.; Vemuri, R.S.; Kaichev, V.V.; Kochubey, V.A.; Saraev, A.A.; Atuchin, V.V. X-ray Photoelectron Spectroscopy Depth Profiling of La₂O₃/Si Thin Films Deposited by Reactive Magnetron Sputtering. *ACS Appl. Mater. Interfaces* **2011**, *3*, 4370–4373. [[CrossRef](#)]
28. Fang, J.; Sun, Y.; Ma, T.; Chen, G.; Wang, L. Preparation of Mn-Ce/TiO₂ Catalysts and its Selective Catalytic Reduction of NO at Low-temperature. *IOP Conf. Series Mater. Sci. Eng.* **2018**, *423*, 012179. [[CrossRef](#)]
29. Huang, J.; Huang, H.; Liu, L.; Jiang, H. Revisit the effect of manganese oxidation state on activity in low-temperature NO-SCR. *Mol. Catal.* **2018**, *446*, 49–57. [[CrossRef](#)]
30. Andreoli, S.P.; Deorsola, F.A.; Galletti, C.; Pirone, R. Nanostructured MnO catalysts for low-temperature NO SCR. *Chem. Eng. J.* **2015**, *278*, 174–182. [[CrossRef](#)]
31. Andreoli, S.; Deorsola, F.A.; Pirone, R. MnO_x-CeO₂ catalysts synthesized by solution combustion synthesis for the low-temperature NH₃-SCR. *Catal. Today* **2015**, *253*, 199–206. [[CrossRef](#)]
32. Xiao, P.; Xuelian, X.; Wang, S.; Zhu, J.; Zhu, Y. One-pot synthesis of LaFeO₃@C composites for catalytic transfer hydrogenation reactions: Effects of carbon precursors. *Appl. Catal. A Gen.* **2020**, *603*, 117742. [[CrossRef](#)]
33. Su, Y.; Fan, B.; Wang, L.; Liu, Y.; Huang, B.; Fu, M.; Chen, L.; Ye, D. MnO_x supported on carbon nanotubes by different methods for the SCR of NO with NH₃. *Catal. Today* **2013**, *201*, 115–121. [[CrossRef](#)]
34. Cheng, S.; Zhang, L.; Xia, H.; Peng, J. Characterization and adsorption properties of La and Fe modified activated carbon for dye wastewater treatment. *Green Process. Synth.* **2017**, *6*, 487–498. [[CrossRef](#)]
35. Yin, S.; Zhu, B.; Sun, Y.; Zi, Z.; Fang, Q.; Li, G.; Chen, C.; Xu, T.; Li, J. Effect of Mn addition on the low-temperature NH₃-selective catalytic reduction of NO_x over Fe₂O₃/activated coke catalysts: Experiment and mechanism. *Asia Pac. J. Chem. Eng.* **2018**, *13*, e2231. [[CrossRef](#)]
36. Eyssler, A.; Winkler, A.; Safonova, O.; Nachtegaal, M.; Matam, S.K.; Hug, P.; Weidenkaff, A.; Ferri, D. On the State of Pd in Perovskite-Type Oxidation Catalysts of Composition A(B,Pd)O_{3±δ} (A = La, Y; B = Mn, Fe, Co). *Chem. Mater.* **2012**, *24*, 1864–1875. [[CrossRef](#)]

37. Li, Z.; Lv, L.; Wang, J.; Ao, X.; Ruan, Y.; Zha, D.; Hong, G.; Wu, Q.; Lan, Y.; Wang, C.; et al. Engineering phosphorus-doped $\text{LaFeO}_{3-\delta}$ perovskite oxide as robust bifunctional oxygen electrocatalysts in alkaline solutions. *Nano Energy* **2018**, *47*, 199–209. [[CrossRef](#)]
38. Hou, X.; Qian, J.; Li, L.; Wang, F.; Li, B.; He, F.; Fan, M.; Tong, Z.; Dong, L.; Dong, L. Preparation and Investigation of Iron–Cerium Oxide Compounds for NO_x Reduction. *Ind. Eng. Chem. Res.* **2018**, *57*, 16675–16683. [[CrossRef](#)]
39. Leelavathi, A.; Madras, G.; Ravishankar, N. Origin of enhanced photocatalytic activity and photoconduction in high aspect ratio ZnO nanorods. *Phys. Chem. Chem. Phys.* **2013**, *15*, 10795. [[CrossRef](#)]
40. Jeong, H.-Y.; Lee, B.-Y.; Lee, Y.-J.; Lee, J.-I.; Yang, M.-S.; Kang, I.-B.; Mativenga, M.; Jang, J. Coplanar amorphous-indium-gallium-zinc-oxide thin film transistor with He plasma treated heavily doped layer. *Appl. Phys. Lett.* **2014**, *104*, 022115. [[CrossRef](#)]
41. Sonsupap, S.; Kidkhunthod, P.; Chanlek, N.; Pinitsoontorn, S.; Maensiri, S. Fabrication, structure, and magnetic properties of electrospun $\text{Ce}_{0.96}\text{Fe}_{0.04}\text{O}_2$ nanofibers. *Appl. Surf. Sci.* **2016**, *380*, 16–22. [[CrossRef](#)]
42. Kim, H.J.; Tak, Y.J.; Park, S.P.; Na, J.W.; Kim, Y.-G.; Hong, S.; Kim, P.H.; Kim, G.T.; Kim, B.K.; Kim, H.J. The self-activated radical doping effects on the catalyzed surface of amorphous metal oxide films. *Sci. Rep.* **2017**, *7*, 12469. [[CrossRef](#)] [[PubMed](#)]
43. Pyeon, M.; Ruoko, T.-P.; LeDuc, J.; Gönüllü, Y.; Deo, M.; Tkachenko, N.V.; Mathur, S. Critical role and modification of surface states in hematite films for enhancing oxygen evolution activity. *J. Mater. Res.* **2018**, *33*, 455–466. [[CrossRef](#)]
44. Li, B.; Raj, A.; Croiset, E.; Wen, J.Z. Reactive Fe–O–Ce Sites in Ceria Catalysts for Soot Oxidation. *Catalysts* **2019**, *9*, 815. [[CrossRef](#)]
45. Wang, T.; Wan, Z.; Yang, X.; Zhang, X.; Niu, X.; Sun, B. Promotional effect of iron modification on the catalytic properties of Mn-Fe/ZSM-5 catalysts in the Fast SCR reaction. *Fuel Process. Technol.* **2018**, *169*, 112–121. [[CrossRef](#)]
46. Zhang, K.; Yu, F.; Zhu, M.; Dan, J.; Wang, X.; Zhang, J.; Dai, B. Enhanced Low Temperature NO Reduction Performance via $\text{MnO}_x\text{-Fe}_2\text{O}_3/\text{Vermiculite}$ Monolithic Honeycomb Catalysts. *Catalysts* **2018**, *8*, 100. [[CrossRef](#)]
47. Yao, X.; Tang, C.; Ji, Z.; Dai, Y.; Cao, Y.; Gao, F.; Dong, L.; Chen, Y. Investigation of the physicochemical properties and catalytic activities of $\text{Ce}_{0.67}\text{M}_{0.33}\text{O}_2$ ($\text{M} = \text{Zr}^{4+}, \text{Ti}^{4+}, \text{Sn}^{4+}$) solid solutions for NO removal by CO. *Catal. Sci. Technol.* **2013**, *3*, 688–698. [[CrossRef](#)]
48. Deng, C.; Li, B.; Dong, L.; Zhang, F.; Fan, M.; Jin, G.; Gao, J.; Gao, L.; Zhang, F.; Zhou, X. NO reduction by CO over CuO supported on CeO_2 -doped TiO_2 : The effect of the amount of a few CeO_2 . *Phys. Chem. Chem. Phys.* **2015**, *17*, 16092–16109. [[CrossRef](#)]
49. Bai, Y.; Bian, X.; Wu, W. Catalytic properties of $\text{CuO/CeO}_2\text{-Al}_2\text{O}_3$ catalysts for low concentration NO reduction with CO. *Appl. Surf. Sci.* **2019**, *463*, 435–444. [[CrossRef](#)]
50. Rosas, J.; Ruiz-Rosas, R.; Rodríguez-Mirasol, J.; Cordero, T. Kinetic study of NO reduction on carbon-supported chromium catalysts. *Catal. Today* **2012**, *187*, 201–211. [[CrossRef](#)]
51. Wu, Y.; Xie, H.; Tian, S.; Tsubaki, N.; Han, Y.; Tan, Y. Isobutanol synthesis from syngas over $\text{K-Cu/ZrO}_2\text{-La}_2\text{O}_3(x)$ catalysts: Effect of La-loading. *J. Mol. Catal. A Chem.* **2015**, *396*, 254–260. [[CrossRef](#)]
52. Liu, T.; Qian, J.; Yao, Y.; Shi, Z.; Han, L.; Liang, C.; Li, B.; Dong, L.; Fan, M.; Zhang, L. Research on SCR of NO with CO over the $\text{Cu}_{0.1}\text{La}_{0.1}\text{Ce}_{0.8}\text{O}$ mixed-oxide catalysts: Effect of the grinding. *Mol. Catal.* **2017**, *430*, 43–53. [[CrossRef](#)]
53. Milt, V.G.; Pissarello, M.; Miró, E.; Querini, C. Abatement of diesel-exhaust pollutants: NO_x storage and soot combustion on $\text{K/La}_2\text{O}_3$ catalysts. *Appl. Catal. B Environ.* **2003**, *41*, 397–414. [[CrossRef](#)]
54. Peralta, M.A.; Zanuttini, M.S.; Ulla, M.; Querini, C. Diesel soot and NO_x abatement on $\text{K/La}_2\text{O}_3$ catalyst: Influence of K precursor on soot combustion. *Appl. Catal. A Gen.* **2011**, *399*, 161–171. [[CrossRef](#)]
55. Lu, P.; Li, C.; Zeng, G.; He, L.; Peng, D.; Cui, H.; Li, S.; Zhai, Y. Low temperature selective catalytic reduction of NO by activated carbon fiber loading lanthanum oxide and ceria. *Appl. Catal. B Environ.* **2010**, *96*, 157–161. [[CrossRef](#)]
56. Cheng, X.; Wang, L.; Wang, Z.; Zhang, M.; Ma, C. Catalytic Performance of NO Reduction by CO over Activated Semicoke Supported Fe/Co Catalysts. *Ind. Eng. Chem. Res.* **2016**, *55*, 12710–12722. [[CrossRef](#)]
57. Spassova, I.; Khristova, M.S.; Panayotov, D.; Mehandjiev, D.R. Coprecipitated CuO-MnO_x Catalysts for Low-Temperature CO–NO and CO–NO– O_2 Reactions. *J. Catal.* **1999**, *185*, 43–57. [[CrossRef](#)]
58. Jiang, X.-Y.; Zhou, R.; Pan, P.; Zhu, B.; Yuan, X.-X.; Zheng, X.-M. Effect of the addition of La_2O_3 on TPR and TPD of $\text{CuO}_y\text{-Al}_2\text{O}_3$ catalysts. *Appl. Catal. A Gen.* **1997**, *150*, 131–141. [[CrossRef](#)]

59. Bîrjega, R.; Pavel, O.; Costentin, G.; Che, M.; Angelescu, E. Rare-earth elements modified hydrotalcites and corresponding mesoporous mixed oxides as basic solid catalysts. *Appl. Catal. A Gen.* **2005**, *288*, 185–193. [[CrossRef](#)]
60. Greluk, M.; Rotko, M.; Turczyniak-Surdacka, S. Enhanced catalytic performance of La₂O₃ promoted Co/CeO₂ and Ni/CeO₂ catalysts for effective hydrogen production by ethanol steam reforming. *Renew. Energy* **2020**, *155*, 378–395. [[CrossRef](#)]
61. Sun, C.; Tang, Y.; Gao, F.; Sun, J.; Ma, K.; Tang, C.; Dong, L. Effects of different manganese precursors as promoters on catalytic performance of CuO-MnO_x/TiO₂ catalysts for NO removal by CO. *Phys. Chem. Chem. Phys.* **2015**, *17*, 15996–16006. [[CrossRef](#)] [[PubMed](#)]

Publisher's Note: MDPI stays neutral with regard to jurisdictional claims in published maps and institutional affiliations.



© 2020 by the authors. Licensee MDPI, Basel, Switzerland. This article is an open access article distributed under the terms and conditions of the Creative Commons Attribution (CC BY) license (<http://creativecommons.org/licenses/by/4.0/>).